American Mineralogist, Volume 83, pages 288–299, 1998

High-pressure single-crystal X-ray diffraction and infrared spectroscopic studies of the $C2/m$-$P2_1/m$ phase transition in cummingtonite

HEXIONG YANG, ROBERT M. HAZEN, CHARLES T. PREWITT, LARRY W. FINGER, REN LU, AND RUSSELL J. HEMLEY

Geophysical Laboratory and Center for High Pressure Research, Carnegie Institution of Washington, 5251 Broad Branch Road, NW, Washington, D.C. 20015-1305, U.S.A.

ABSTRACT

The structural changes associated with the $C2/m$-$P2_1/m$ phase transition in cummingtonite with (Fe + Mn)/(Fe + Mn + Mg) ≈ 0.50 have been studied with single-crystal X-ray diffraction at various pressures up to 7.90 GPa and infrared spectroscopy up to 8.63 GPa. With increasing pressure, the crystal transforms from $C2/m$ to $P2_1/m$ symmetry at ~1.21 GPa, as determined by the appearance of reflections violating the $C2/m$ space group. Infrared spectra provide additional evidence for the phase transition: A distinct splitting of OH stretching bands results from an increase from one to two nonequivalent OH positions. The $C2/m$-$P2_1/m$ transition is of weakly displacive first-order or tricritical character with apparent slope changes in the plots of the axial ratios a/b and a/c as a function of pressure. The unit-cell compression is considerably anisotropic with the a dimension in both $C2/m$ and $P2_1/m$ phases being the most compressible. Major structural changes for the $C2/m$-$P2_1/m$ transition include: (1) One crystallographically distinct silicate chain becomes two discontinuously, coupled by the splitting of the M4-O5 bond, as well as M4-O6, into two nonequivalent bonds, and (2) the M4-cation coordination increases from sixfold to sevenfold. More importantly, we observed a change in the sense of rotation for the A chain while the crystal structure maintains $P2_1/m$ symmetry: It is O rotated, as the B chain, at 1.32 GPa, but S-rotated at 2.97 GPa and higher pressures. As pressure increases from 1.32 to 7.90 GPa, there is a switching of the nearest bridging O atoms coordinated with the M4 cation: The M4-O5B distance contracts from 2.944 to 2.551 Å, whereas the M4-O6B distance increases from 2.754 to 2.903 Å. Compression mechanisms for the low- and high-pressure polymorphs appear to be slightly different. In the $C2/m$ phase, the behavior of the A and M4 sites controls the compression of the structure, whereas the response of the M1, M2, and M3 octahedra to pressure also plays a role in determining the compression of the $P2_1/m$ structure. The phase transition is regarded as primarily driven by the differential compression between the M4 and T sites, and the symmetry breaking provides a necessary tighter coordination for the M4 site. Based on our data, the obvious changes in the hyperfine parameters of ^{57}Fe in grunerite between 1.0 and 3.4 GPa, observed by Zhang and Hafner (1992), are likely to result from the $C2/m$-$P2_1/m$ structural transformation.

INTRODUCTION

Cummingtonite, $(Mg,Fe)_7Si_8O_{22}(OH)_2$, is an important ferromagnesian amphibole that occurs in a wide variety of metamorphic and igneous rocks. It may crystallize in two distinct polymorphs: one with the space group $C2/m$ and the other $P2_1/m$. $P2_1/m$ cummingtonite is generally restricted to Mg-rich compositions (Hirschmann et al. 1994 and references therein) and is considered to represent an important link between the two most abundant amphibole structure types, the monoclinic $C2/m$ and the orthorhombic $Pbnm$ structures (Ross et al. 1968, 1969; Papike et al. 1969; Prewitt et al. 1970; Maresch and Czank 1988). The crystal structures of both $P2_1/m$ and $C2/m$ cummingtonites are characterized by double silicate chains running parallel to c, each chain consisting of two nonequivalent SiO_4 tetrahedra, T1 and T2. The silicate chains are linked together along [100] by cations occupying four different octahedral sites M1, M2, M3, and M4. The two structures differ in two major aspects. One is that the $C2/m$ structure contains one crystallographically distinct O-rotated silicate chain, whereas the $P2_1/m$ structure contains two, designated as the S-rotated A chain and O-rotated B chain (Yang and Hirschmann 1995; for illustration of S and O rotations, see Fig. 1 of Papike and Ross 1970). The other is that the respective site symmetries of M1, M2, M3, and M4 are 2, 2, $2/m$, and 2 for the $C2/m$ structure, but 1, 1, m, and 1 for the $P2_1/m$ structure. Amphibole structures have been reviewed by Papike

0003–004X/98/0304–0288$05.00

TABLE 1. Crystal data and relevant information on cummingtonite at various pressures

Pressure (GPa)	a (Å)	b (Å)	c (Å)	β (°)	V (Å³)	Refls. $>3\sigma_I$	Refl. violating C2/m S.G.	R_{int}	R_w	R	Space group
0.00*	9.5220(6)	18.1833(7)	5.3184(6)	102.020(7)	900.66(10)	1480			0.029	0.024	C2/m
0.00†	9.5231(9)	18.1817(12)	5.3185(6)	102.028(10)	900.66(13)	461		0.027	0.063	0.059	C2/m
0.60†	9.4890(5)	18.1508(9)	5.3102(3)	102.210(6)	893.89(9)	454		0.028	0.063	0.058	C2/m
1.10†	9.4638(9)	18.1333(11)	5.3022(5)	102.372(10)	888.79(12)	458		0.029	0.063	0.062	C2/m
1.32†	9.4498(7)	18.1083(11)	5.2978(5)	102.417(8)	885.34(11)	560	42	0.029	0.057	0.056	$P2_1/m$
1.76	9.4326(6)	18.0839(9)	5.2900(4)	102.493(8)	880.98(11)						
2.97†	9.3798(8)	18.0075(11)	5.2659(5)	102.723(10)	867.60(13)	633	142	0.031	0.058	0.054	$P2_1/m$
4.05	9.3383(9)	17.9474(10)	5.2480(4)	102.864(10)	857.48(11)						
5.09†	9.2993(9)	17.8900(12)	5.2321(4)	102.979(10)	848.19(13)	806	231	0.033	0.055	0.053	$P2_1/m$
6.27	9.2608(8)	17.8285(11)	5.2146(4)	103.063(10)	838.69(13)						
7.90†	9.2099(8)	17.7605(9)	5.1930(4)	103.173(9)	827.08(11)	730	250	0.036	0.061	0.058	$P2_1/m$

* X-ray intensity data were collected in air.
† X-ray intensity data were collected at these pressures.

and Ross (1970), Cameron and Papike (1979), Law and Whittaker (1980), Chisholm (1981), and Hawthorne (1983).

Ross et al. (1968, 1969) suggested that $P2_1/m$ cummingtonite is the amphibole analog of pigeonite and would undergo a $P2_1/m$-$C2/m$ phase transition at high temperature. Prewitt et al. (1970), using in-situ high-temperature X-ray precession photography, found that a $P2_1/m$ manganoan cummingtonite crystal with X_{Fe} [= (Fe + Mn)/(Fe + Mn + Mg)] ≈ 0.15 inverts to the $C2/m$ structure at ~45 °C, and that the transition is reversible and unquenchable. From high-temperature single-crystal X-ray diffraction data, Sueno et al. (1972) showed that the $P2_1/m$-$C2/m$ transition in the same sample takes place at ~100 °C and refined the crystal structure of the $C2/m$ phase at 270 °C. Yang and Smyth (1996) reported that a cummingtonite crystal with X_{Fe} = 0.37 transforms from $C2/m$ symmetry at room temperature to $P2_1/m$ symmetry at −33 °C and refined the $P2_1/m$ structure at −133 °C.

It has been generally agreed that the effective M4-cation size, which can be affected by temperature and the Mg/Fe site occupancy, plays a critical role in the relative stabilities of the $C2/m$ and $P2_1/m$ structures. However, due to the lack of systematic structural data as a function of temperature and pressure, the nature (first- or higher order) and mechanism of the phase transformation in cummingtonite are still not well understood. From the crystal-chemistry point of view, of particular interest are how the S-rotated A chain and O-rotated B chain in the $P2_1/m$ structure become identical in the $C2/m$ structure and whether or not the A and B chains can possess the same sense of rotation in the $P2_1/m$ phase. In this paper, we report the results of a single-crystal X-ray structure study of cummingtonite with X_{Fe} = 0.50 as a function of pressure across the $P2_1/m$-$C2/m$ transition to gain insights into detailed structural changes associated with the phase transformation.

EXPERIMENTAL PROCEDURES

Room-pressure X-ray diffraction data measurements

The cummingtonite sample (DH7-484) used in this study is from Bloom Lake, Quebec, and was kindly supplied by B.W. Evans of the University of Washington. Its locality and chemical composition were first described by Mueller (1960). Hirschmann et al. (1994) performed X-ray structure refinements on five crystals from this sample: an unheated crystal, two heat-treated ones at 600 °C, and two at 700 °C. The sample has $C2/m$ symmetry at ambient conditions and the chemical composition (average of five crystals) is $(Ca_{0.076}Mg_{3.445}Fe_{3.272}Mn_{0.199}Al_{0.008})(Si_{7.983}Al_{0.017})O_{22}(OH)_2$ (Hirschmann et al. 1994). A single-crystal fragment (0.10 × 0.09 × 0.04 mm) showing sharp diffraction profiles was selected from a crushed sample for the study. A Picker four-circle diffractometer equipped with a Mo X-ray tube (β-filtered) was used for all X-ray diffraction measurements. Unit-cell parameters were determined by fitting the positions of 16 reflections with $20° < 2\theta < 35°$ following the procedure of King and Finger (1979). The values (Table 1) are very close to those reported by Hirschmann et al. (1994) for the same unheated material: a = 9.520(1), b = 18.185(1), c = 5.3195(5) Å, β = 102.002(2)°, and V = 900.79 Å³.

X-ray diffraction intensity data from one quadrant of reciprocal space with $0° \le 2\theta \le 60°$ were collected on the basis of the primitive lattice using ω scans of 1° width in step increments of 0.025° and 2 s per step counting time. Digitized step data were integrated by the method of Lehmann and Larsen (1974) with background manually reset when necessary. Corrections were made for Lorentz and polarization effects and for X-ray absorption by the crystal (μ = 30.18 cm⁻¹). Reflections having intensities greater than $2\sigma_I$ were considered as observed and included in the refinement, where σ_I is the standard deviation determined from the counting statistics. Out of 1490 observed reflections, seven weak ones [$I < 5\ \sigma_I$] violate $C2/m$ symmetry; these reflections probably originate from microscopic exsolution lamellae of actinolite (Hirschmann et al. 1994) or chain-width disorder (e.g., Veblen 1985; Maresch and Czank 1988).

The initial structural model of cummingtonite was taken from Hirschmann et al. (1994). Least-squares refinements were carried out using an updated version of RFINE4 (Finger and Prince 1975) in the $C2/m$ space

TABLE 2. Atomic positional coordinates and isotropic displacement parameters of cummingtonite at various pressures

				1.32		2.97	
P (GPa)	0.00	0.60	1.10	Set A	Set B	Set A	Set B
M1 *x*	0	0	0	−0.2458(9)		−0.2491(5)	
M1 *y*	0.0874(2)	0.0871(1)	0.0869(2)	0.3370(1)		0.3367(1)	
M1 *z*	0.5	0.5	0.5	0.4938(11)		0.4858(6)	
M1 *B*	0.75(5)	0.69(4)	0.76(5)	0.66(5)		0.72(4)	
M2 *x*	0	0	0	−0.2521(11)		−0.2510(7)	
M2 *y*	0.1776(2)	0.1776(2)	0.1770(2)	0.4268(2)		0.4262(2)	
M2 *z*	0	0	0	0.9940(13)		0.9837(9)	
M2 *B*	0.78(5)	0.71(5)	0.65(5)	0.73(5)		0.74(5)	
M3 *x*	0	0	0	−0.2516(10)		−0.2477(10)	
M3 *y*	0	0	0	0.25		0.25	
M3 *z*	0	0	0	0.9895(12)		0.9873(11)	
M3 *B*	0.61(6)	0.70(6)	0.71(7)	0.64(7)		0.70(7)	
M4 *x*	0	0	0	−0.2604(6)		−0.2564(4)	
M4 *y*	0.2592(1)	0.2590(1)	0.2591(1)	0.5093(1)		0.5101(1)	
M4 *z*	0.5	0.5	0.5	0.4841(8)		0.4793(4)	
M4 *B*	0.93(4)	0.92(4)	0.90(4)	0.78(5)		0.89(3)	
T1 *x*	0.2865(3)	0.2883(2)	0.2890(2)	0.0430(11)	0.5352(11)	0.0417(6)	0.5426(6)
T1 *y*	0.0841(1)	0.0840(1)	0.0840(1)	0.3364(6)	0.8315(6)	0.3345(3)	0.8335(3)
T1 *z*	0.2735(3)	0.2757(3)	0.2764(3)	0.2768(13)	0.2768(14)	0.2633(8)	0.2960(7)
T1 *B*	0.67(4)	0.60(4)	0.61(4)	0.60(9)	0.51(8)	0.71(7)	0.52(7)
T2 *x*	0.2972(3)	0.2978(3)	0.2979(2)	0.0516(14)	0.5453(14)	0.0465(6)	0.5525(6)
T2 *y*	0.1685(1)	0.1686(1)	0.1686(1)	0.4198(7)	0.9175(7)	0.4204(3)	0.9169(3)
T2 *z*	0.7800(3)	0.7818(4)	0.7823(3)	0.7808(16)	0.7847(15)	0.7705(8)	0.8017(8)
T2 *B*	0.60(4)	0.63(3)	0.68(4)	0.65(10)	0.74(10)	0.67(8)	0.66(8)
O1 *x*	0.1139(6)	0.1160(6)	0.1179(6)	−0.1353(24)	0.3683(23)	−0.1297(16)	0.3666(14)
O1 *y*	0.0875(3)	0.0871(3)	0.0871(3)	0.3395(13)	0.8343(13)	0.3359(8)	0.8375(7)
O1 *z*	0.2070(7)	0.2096(7)	0.2105(9)	0.2194(25)	0.2022(25)	0.2012(17)	0.2207(18)
O1 *B*	0.76(11)	0.79(9)	0.62(9)	0.73(21)	0.66(23)	1.24(21)	0.56(19)
O2 *x*	0.1243(7)	0.1266(6)	0.1276(6)	−0.1279(12)	0.3811(23)	−0.1284(13)	0.3820(14)
O2 *y*	0.1729(3)	0.1724(3)	0.1727(3)	0.4253(12)	0.9198(12)	0.4218(6)	0.9218(7)
O2 *z*	0.7181(8)	0.7202(7)	0.7220(9)	0.7101(16)	0.7315(23)	0.7014(14)	0.7413(16)
O2 *B*	0.90(11)	0.69(10)	0.83(10)	0.56(26)	0.62(25)	0.56(21)	1.03(23)
O3 *x*	0.1181(11)	0.1166(9)	0.1174(9)	−0.1176(28)	0.3574(28)	−0.1234(20)	0.3674(17)
O3 *y*	0	0	0	0.25	0.75	0.25	0.75
O3 *z*	0.7081(11)	0.7093(11)	0.7079(12)	0.7216(35)	0.6985(34)	0.7034(25)	0.7261(23)
O3 *B*	0.87(15)	0.80(13)	0.89(13)	0.76(30)	0.66(31)	1.25(31)	0.57(28)
O4 *x*	0.3808(6)	0.3807(6)	0.3801(6)	0.1327(28)	0.6262(27)	0.1284(15)	0.6314(15)
O4 *y*	0.2450(3)	0.2451(3)	0.2454(3)	0.4961(13)	0.9953(13)	0.4991(6)	0.9927(7)
O4 *z*	0.7682(7)	0.7675(7)	0.7663(7)	0.7701(26)	0.7639(26)	0.7789(17)	0.7584(16)
O4 *B*	0.95(10)	1.07(10)	1.08(11)	1.11(22)	1.19(24)	0.79(23)	1.15(20)
O5 *x*	0.3518(7)	0.3527(6)	0.3534(7)	0.1059(15)	0.5976(16)	0.1079(11)	0.6028(11)
O5 *y*	0.1302(4)	0.1309(3)	0.1314(3)	0.3774(8)	0.8862(8)	0.3737(6)	0.8896(6)
O5 *z*	0.0622(8)	0.0640(7)	0.0677(8)	0.0463(18)	0.0833(20)	0.0365(14)	0.0993(14)
O5 *B*	0.86(11)	0.85(10)	0.83(9)	0.69(18)	0.75(19)	0.74(15)	0.47(15)
O6 *x*	0.3504(6)	0.3524(6)	0.3530(6)	0.1025(16)	0.6065(16)	0.1095(13)	0.6031(11)
O6 *y*	0.1190(4)	0.1184(3)	0.1182(3)	0.3744(8)	0.8615(8)	0.3777(6)	0.8589(6)
O6 *z*	0.5558(7)	0.5607(7)	0.5625(8)	0.5489(19)	0.5796(19)	0.5346(15)	0.5978(14)
O6 *B*	1.17(11)	1.24(10)	1.17(11)	0.93(23)	1.08(25)	0.97(16)	0.99(18)
O7 *x*	0.3433(10)	0.3432(11)	0.3447(9)	0.0909(25)	0.6027(25)	0.0985(17)	0.6051(18)
O7 *y*	0	0	0	0.25	0.75	0.25	0.75
O7 *z*	0.2723(12)	0.2694(14)	0.2709(11)	0.2880(29)	0.2526(31)	0.2938(20)	0.2587(23)
O7 *B*	0.94(14)	1.02(14)	0.72(12)	0.64(26)	0.54(24)	0.49(22)	0.85(24)

group. The structure was refined with the bulk composition constrained to that determined from microprobe analysis. Procedures of the structure refinement were similar to those described by Hirschmann et al. (1994). Weighting schemes were based on $w = [\sigma^2(F) + (pF)^2]^{-1}$, where p is adjusted to ensure that the errors were normally distributed through probability plot analysis (Ibers and Hamilton 1974). Type II isotropic extinction corrections (Becker and Coppens 1975) were applied in the refinements. Because of their similar X-ray scattering power, Fe and Mn were grouped together and the scattering factors for Fe were used in the refinement. The determined site occupancies for the four M sites are as follows: M1: Fe = 0.405(3), Mg = 0.595; M2: Fe = 0.207(3), Mg = 0.789, Al = 0.004; M3: Fe = 0.393(4), Mg = 0.607; M4: Fe = 0.927, Mg = 0.035, Ca = 0.038. Considering the experimental errors, these values are comparable with those obtained by Hirschmann et al. (1994) [M1: Fe = 0.393 (6), Mg = 0.607; M2: Fe = 0.214(6), Mg = 0.782, Al = 0.004; M3: Fe = 0.400(9), Mg = 0.600; M4: Fe = 0.924, Mg = 0.044, Ca = 0.032]. Atomic positional coordinates and anisotropic displacement parameters at room pressure are available upon request.

High-pressure X-ray diffraction data measurements

The same crystal was mounted in a modified Merrill-Bassett diamond-anvil cell with a mixture of 4:1 methanol and ethanol as the pressure medium. Four small (~10

TABLE 2—*Extended*

	5.09		7.90	
P (GPa)	Set A	Set B	Set A	Set B
M1 *x*	−0.2497(5)		−0.2510(4)	
M1 *y*	0.3364(1)		0.3359(1)	
M1 *z*	0.4800(5)		0.4736(6)	
M1 *B*	0.57(4)		0.59(4)	
M2 *x*	−0.2522(5)		−0.2516(6)	
M2 *y*	0.4253(2)		0.4249(2)	
M2 *z*	0.9785(6)		0.9756(7)	
M2 *B*	0.77(5)		0.64(5)	
M3 *x*	−0.2492(7)		−0.2489(7)	
M3 *y*	0.25		0.25	
M3 *z*	0.9829(9)		0.9755(9)	
M3 *B*	0.71(6)		0.62(6)	
M4 *x*	−0.2577(3)		−0.2602(3)	
M4 *y*	0.5107(1)		0.5107(1)	
M4 *z*	0.4715(4)		0.4657(3)	
M4 *B*	0.68(4)		0.67(3)	
T1 *x*	0.0434(5)	0.5464(5)	0.0454(5)	0.5502(5)
T1 *y*	0.3347(2)	0.8330(2)	0.3342(2)	0.8329(2)
T1 *z*	0.2591(6)	0.3051(7)	0.2561(7)	0.3118(7)
T1 *B*	0.56(6)	0.70(6)	0.54(6)	0.68(6)
T2 *x*	0.0461(5)	0.5545(5)	0.0458(5)	0.5558(5)
T2 *y*	0.4208(2)	0.9167(2)	0.4214(2)	0.9163(2)
T2 *z*	0.7656(6)	0.8084(7)	0.7618(7)	0.8132(7)
T2 *B*	0.72(6)	0.63(6)	0.59(6)	0.61(6)
O1 *x*	−0.1322(12)	0.3700(11)	−0.1305(12)	0.3724(11)
O1 *y*	0.3356(5)	0.8370(5)	0.3360(5)	0.8361(5)
O1 *z*	0.1933(13)	0.2262(13)	0.1873(17)	0.2344(14)
O1 *B*	1.03(18)	0.81(17)	0.82(13)	0.68(14)
O2 *x*	−0.1259(12)	0.3790(13)	−0.1283(12)	0.3821(12)
O2 *y*	0.4215(4)	0.9211(5)	0.4210(5)	0.9208(5)
O2 *z*	0.6986(15)	0.7446(16)	0.6968(13)	0.7480(16)
O2 *B*	0.55(15)	0.68(15)	0.79(13)	0.81(13)
O3 *x*	−0.1292(14)	0.3743(14)	−0.1251(15)	0.3728(15)
O3 *y*	0.25	0.75	0.25	0.75
O3 *z*	0.6951(17)	0.7300(18)	0.6896(19)	0.7367(19)
O3 *B*	0.75(18)	0.83(19)	0.71(17)	0.76(18)
O4 *x*	0.1241(10)	0.6333(11)	0.1222(12)	0.6322(11)
O4 *y*	0.4993(4)	0.9933(4)	0.5022(4)	0.9932(5)
O4 *z*	0.7863(13)	0.7536(14)	0.7859(14)	0.7545(15)
O4 *B*	0.79(14)	0.67(13)	0.53(13)	0.83(13)
O5 *x*	0.1096(10)	0.6098(10)	0.1117(11)	0.6100(10)
O5 *y*	0.3718(4)	0.8918(4)	0.3692(5)	0.8930(5)
O5 *z*	0.0281(12)	0.1170(12)	0.0176(14)	0.1259(14)
O5 *B*	0.81(14)	0.63(14)	0.96(13)	0.90(12)
O6 *x*	0.1126(9)	0.6038(10)	0.1134(11)	0.6093(11)
O6 *y*	0.3817(4)	0.8561(4)	0.3842(5)	0.8527(4)
O6 *z*	0.5277(11)	0.6099(12)	0.5194(14)	0.6215(14)
O6 *B*	0.76(13)	0.91(14)	0.75(12)	0.59(13)
O7 *x*	0.1066(14)	0.6057(14)	0.1118(15)	0.6091(15)
O7 *y*	0.25	0.75	0.25	0.75
O7 *z*	0.3033(16)	0.2616(16)	0.3141(19)	0.2542(18)
O7 *B*	0.96(16)	0.75(18)	0.93(18)	0.44(18)

μm) ruby chips were included as the internal pressure calibrant (Mao et al. 1986), from which pressure was determined from the position of the R_1 laser-induced fluorescence peak, with an error of approximately 0.05 GPa. The fixed-ϕ mode of data measurement (Finger and King 1978) was employed throughout the high-pressure experiments to maximize reflection accessibility and minimize attenuation by the diamond cell. Lattice parameters were determined using the same method as described for the room-pressure experiment.

To ensure that the crystal has $P2_1/m$ symmetry at high pressure, the pressure of the crystal was raised to 7.90 GPa and all X-ray diffraction measurements were made during decompression. The four strongest reflections violating the $C2/m$ space group ($h + k = 2n + 1$) ($\bar{1}63$, $\bar{3}02$, $\bar{1}04$, and $\bar{3}65$) were selected from the X-ray diffraction data of Yang and Smyth (1996) to monitor the phase transition. These reflections are hereafter referred to as primitive reflections. The intensities and peak profiles of these primitive reflections were measured immediately after the unit-cell dimension determination at each pressure. No significant broadening of the primitive reflections was observed with decreasing pressure. All primitive reflections disappeared when pressure was released from 1.32 to 1.10 GPa. For a better comparison with high-pressure data, another set of room-pressure X-ray intensity data was collected while the crystal was still mounted in the diamond-anvil cell. After the data collection at room pressure, the pressure of the crystal was gradually raised again to check the reversibility of the phase transition; the primitive reflections reappeared between 1.00 and 1.15 GPa.

X-ray diffraction intensity data were collected for all accessible reflections with $0° \leq 2\theta \leq 60°$. The intensity data above 1.32 GPa were collected based on $P2_1/m$ symmetry and those below 1.10 GPa on $C2/m$ symmetry. The experimental procedures for X-ray data collection, reduction, and structure refinements were similar to those described above, but only atomic isotropic displacement factors were refined. In addition, corrections were made for absorption by the diamond and beryllium components of the pressure cell and the Fe-Mg distribution among the four M sites was assumed to be the same as that determined from the room-pressure data collected without the diamond-anvil cell. Unit-cell dimensions and final refinement statistics are given in Table 1; atomic positional and isotropic displacement parameters are listed in Table 2; selected interatomic distances and angles are presented in Tables 3 and 4, respectively. Polyhedral volumes and distortion indices are given in Table 5.

High-pressure infrared spectroscopy

Infrared spectroscopy is an ideal probe of local structural and symmetry environments and is especially useful for detecting minor structural changes, such as those involving H positions. To gain an insight into the changes in the H environments in cummingtonite across the $C2/m$-$P2_1/m$ transformation, we carried out an infrared spectroscopic study on the same cummingtonite sample (DH7-484) at various pressures up to 8.63 GPa. Infrared absorption spectra were obtained with a Bruker IFS66Vs Fourier transform interferometer equipped with a Bruker II microscope and conventional (globar) light source. A KBr beam splitter and a liquid nitrogen-cooled HgCdTe (MCT) detector were used. The spectrometer bench was evacuated and the microscope was purged with nitrogen gas. A recently developed symmetrical piston-cylinder diamond anvil cell (Mao and Hemley 1996) with type I diamonds, together with KBr as pressure medium and ruby as pressure calibrant, was used. Infrared data were collected at 2 cm^{-1} resolution. A single-crystal fragment of ~0.05 × 0.05 × 0.02 mm was placed slightly off the

TABLE 3. Selected interatomic distances (Å) for cummingtonite at various pressures

				1.32		2.97		5.09		7.90	
P (GPa)	0.00	0.60	1.10	Set A	Set B	Set A	Set B	Set A	Set B	Set A	Set B
M1-O1	2.076(5)	2.076(5)	2.082(5)	1.964(19)	2.177(18)	2.059(12)	2.087(11)	2.045(12)	2.095(12)	2.048(10)	2.079(9)
M1-O2	2.143(6)	2.148(5)	2.156(6)	2.136(18)	2.157(20)	2.086(11)	2.162(12)	2.088(9)	2.118(10)	2.076(9)	2.103(10)
M1-O3	2.120(6)	2.107(5)	2.099(6)	2.186(16)	2.042(15)	2.132(11)	2.090(10)	2.085(11)	2.090(11)	2.083(8)	2.054(8)
Avg.	2.113	2.110	2.112	2.110		2.103		2.087		2.074	
M2-O1	2.139(6)	2.152(6)	2.148(6)	2.139(22)	2.145(22)	2.162(14)	2.091(13)	2.126(11)	2.077(11)	2.094(10)	2.088(10)
M2-O2	2.097(5)	2.101(5)	2.095(5)	2.098(13)	2.093(19)	2.072(11)	2.097(12)	2.074(11)	2.065(11)	2.035(10)	2.073(10)
M2-O4	2.051(6)	2.045(6)	2.049(6)	2.044(23)	2.048(22)	2.015(12)	2.045(13)	2.023(10)	2.019(10)	1.989(9)	2.005(10)
Avg.	2.095	2.099	2.097	2.095		2.080		2.065		2.047	
M3-O1	2.103(5)	2.105(5)	2.110(5)	2.178(22)	2.024(22)	2.083(14)	2.095(13)	2.050(11)	2.081(11)	2.046(10)	2.063(10)
M3-O3	2.098(8)	2.081(7)	2.091(7)	2.095(24)	2.108(22)	2.089(17)	2.070(15)	2.066(16)	2.096(17)	2.068(13)	2.077(13)
Avg.	2.101	2.097	2.103	2.101		2.086		2.071		2.060	
M4-O2	2.153(6)	2.165(5)	2.164(6)	2.161(17)	2.161(20)	2.172(11)	2.159(12)	2.192(9)	2.132(10)	2.188(9)	2.115(9)
M4-O4	2.001(5)	1.996(5)	1.994(5)	1.995(21)	2.009(20)	2.009(12)	1.988(11)	2.037(11)	1.971(10)	2.033(9)	1.978(9)
M4-O6	2.683(7)	2.685(6)	2.682(6)	2.609(15)	2.754(15)	2.456(12)	2.838(11)	2.350(9)	2.878(9)	2.296(10)	2.903(8)
M4-O5	3.176(6)	3.153(5)	3.124(5)	3.312(13)	2.944(13)	3.355(9)	2.801(10)	3.399(9)	2.641(9)	3.457(8)	2.551(8)
Avg. 6	2.279	2.282	2.280	2.282		2.270		2.260		2.252	
Avg. 8	2.503	2.500	2.491	2.493		2.473		2.450		2.440	
T1-O1	1.609(6)	1.599(6)	1.583(6)	1.648(24)	1.542(24)	1.569(16)	1.612(14)	1.592(15)	1.601(15)	1.578(12)	1.596(11)
T1-O5	1.626(6)	1.629(5)	1.620(5)	1.646(14)	1.625(16)	1.624(10)	1.634(10)	1.617(10)	1.638(9)	1.624(9)	1.618(9)
T1-O6	1.627(5)	1.631(4)	1.631(5)	1.587(14)	1.691(13)	1.628(10)	1.631(9)	1.640(9)	1.618(10)	1.631(9)	1.615(8)
T1-O7	1.622(4)	1.614(4)	1.614(3)	1.626(13)	1.624(14)	1.609(7)	1.641(8)	1.623(7)	1.618(8)	1.618(6)	1.620(6)
Avg.	1.621	1.618	1.612	1.627	1.620	1.607	1.630	1.618	1.619	1.613	1.612
T2-O2	1.612(7)	1.589(6)	1.580(6)	1.660(17)	1.517(25)	1.600(13)	1.563(14)	1.559(13)	1.592(13)	1.561(12)	1.560(12)
T2-O4	1.610(6)	1.606(6)	1.606(6)	1.587(27)	1.618(27)	1.608(13)	1.593(14)	1.573(9)	1.610(9)	1.591(9)	1.597(10)
T2-O5	1.638(5)	1.629(5)	1.637(5)	1.588(15)	1.653(14)	1.627(10)	1.611(9)	1.625(9)	1.642(9)	1.620(9)	1.640(8)
T2-O6	1.655(6)	1.654(5)	1.651(5)	1.634(16)	1.677(17)	1.675(11)	1.641(10)	1.663(10)	1.637(10)	1.663(9)	1.653(8)
Avg.	1.629	1.620	1.619	1.617	1.616	1.628	1.602	1.605	1.620	1.609	1.612

center in the gasket hole so that a reference spectrum could be obtained at each pressure to remove the absorption from remnant H_2O and CO_2 in the IR beam path.

RESULTS AND DISCUSSION

Phase-transition pressure in cummingtonite

At 7.90 GPa, the four monitored primitive reflections had strong intensities and sharp peak shapes. With decreasing pressure, the peak profiles of these reflections remained sharp, but their intensities decreased appreciably and became undetectable between 1.32 and 1.10 GPa. The phase-transition pressure (P_{tr}) is thus estimated to be at 1.21 ± 0.11 GPa, which is consistent with that (between 1.04 and 1.54 GPa) determined from the high-pressure infrared spectrum measurements on the same sample (see below). The *C*2/*m*-*P*2$_1$/*m* transition is reversible, in agreement with Prewitt et al. (1970) and Yang and Smyth (1996). Given the experimental uncertainties, the hysteresis associated with the transition is not obvious. This result is compared to the *P*2$_1$/*c*-*C*2/*c* inversion in clinopyroxene. Prewitt et al. (1971) and Brown et al. (1972) observed a hysteresis effect of the transition in Ca-rich pigeonite, whereas Smyth and Burnham (1972) reported no hysteresis in Ca-poor clinopyroxene.

Yang and Hirschmann (1995) reported that the relative stability of *P*2$_1$/*m* vs. *C*2/*m* cummingtonite depends on the bulk composition (X_{Fe}), as well as the Mg occupancy in the M4 site: An increase in X_{Fe} stabilizes the *C*2/*m* structure, but destabilizes the *P*2$_1$/*m* structure. Accordingly, it follows that the *C*2/*m*-*P*2$_1$/*m* transition pressure increases as cummingtonite becomes more Fe-rich. To better constrain the relationship between bulk composition and the *C*2/*m*-*P*2$_1$/*m* transition pressure in cummingtonite and grunerite, we also determined the phase-transition pressure for an Fe-rich (X_{Fe} = 0.89) grunerite sample (labeled as 1-K), whose structure has been well characterized (Finger 1969; Hirschmann et al. 1994). The examined crystal transformed from *C*2/*m* to *P*2$_1$/*m* symmetry at 2.60 ± 0.15 GPa. By assuming a linear dependence of the *C*2/*m*-*P*2$_1$/*m* transition pressure on X_{Fe} and that the

TABLE 4. Selected bond angles in cummingtonite at various pressures

				1.32		2.97		5.09		7.90	
Angle (°)	0.00	0.60	1.10	Set A	Set B	Set A	Set B	Set A	Set B	Set A	Set B
O5-O6-O5	171.2(4)	170.2(3)	169.7(3)	177.3(9)	160.5(9)	176.8(7)	156.3(6)	172.2(5)	152.5(4)	168.3(6)	149.2(5)
O5-O7-O6	170.4(3)	169.0(3)	168.7(3)	174.5(1.0)	159.3(7)	174.8(7)	156.0(5)	172.5(6)	152.9(5)	168.0(4)	148.5(4)
T1-O5-T2	139.3(4)	139.5(4)	139.2(4)	140.9(1.0)	137.6(1.0)	137.6(7)	137.5(7)	136.6(8)	133.6(7)	135.1(7)	133.6(6)
T1-O6-T2	139.9(4)	139.3(4)	139.2(4)	142.8(1.1)	133.3(1.0)	137.4(8)	136.7(7)	135.8(7)	135.8(7)	135.4(7)	132.0(6)
T1-O7-T1	141.0(6)	141.7(7)	141.4(6)	148.3(1.7)	130.7(1.6)	142.2(1.0)	132.7(1.0)	138.0(1.2)	133.2(1.1)	135.2(9)	130.6(9)

$P2_1/m$ polymorph is only stable with $X_{Fe} < 0.33$ (Yang and Hirschmann 1995), we have $P_{tr} = -1.23 + 4.52\ X_{Fe}$ (Fig. 1). Based on these data, the grunerite sample ($X_{Fe} = 0.78$) studied by Zhang and Hafner (1992) and Zhang et al. (1992) would have undergone the $C2/m$-$P2_1/m$ phase transformation at ~2.43 GPa, and the obvious change in the hyperfine parameters of ^{57}Fe between 1.0 and 3.4 GPa, observed by Zhang and Hafner (1992), is likely to result from the $C2/m$-$P2_1/m$ structural transition.

Unit-cell compressibilities and bulk moduli

The $C2/m$-$P2_1/m$ phase transition in cummingtonite is associated with a small but discernible slope change in *a*, *b*, and *c*, with an increase in the slope for *a* and a decrease for *b* and *c*, suggesting a change in the compression mechanism. The slope changes can be better visualized in the plots of *a*/*b* and *a*/*c* vs. pressure (Fig. 2). No apparent slope change was found for β and the unit-cell volume *V* within the experimental errors. Both $C2/m$ and $P2_1/m$ structures exhibit strong compression anisotropy with the most compressible direction along [100]. The linear compressibilities along [100] (β_a), *b* (β_b), and *c* (β_c) are 0.0068(2), 0.0024(3), and 0.0028(1) GPa^{-1}, respectively, for the $C2/m$ phase, and 0.0043(3), 0.0029(1), and 0.0030(1) GPa^{-1} for the $P2_1/m$ phase. Thus, the phase transition is accompanied by a significant decrease in β_a and a slight increase in β_b and β_c, resulting in a great reduction in the compression anisotropy for the $P2_1/m$ structure. The axial compression ratios (β_a:β_b:β_c) are 2.83:1.00:1.17 for the $C2/m$ polymorph and 1.48:1.00:1.03 for the $P2_1/m$ polymorph. From single-crystal X-ray diffraction data, Zhang et al. (1992) obtained β_a:β_b:β_c = 1.42:1.00:1.03 for a grunerite crystal with $X_{Fe} = 0.78$, which is very comparable with our data. Although Zhang et al. (1992) claimed that they did not observe any anomaly in their unit-cell dimensions vs. pressure, their plots of *a*/*b* and *a*/*c* against pressure (Fig. 2) do display a noticeable slope change between 1.7 and 2.7 GPa, suggesting that their crystal underwent the $C2/m$-$P2_1/m$ transition between 1.7 and 2.7 GPa.

Weighted volume and pressure data fit to a second-order Birch-Murnaghan equation of state produces V_0 = 900.66(2) Å^3 and K_0 = 78(3) GPa ($K' \equiv 4.0$) for the $C2/m$ phase and V_0 = 900.66(2) Å^3, K_0 = 71(1) GPa, and K' = 6.1(5) for the $P2_1/m$ phase. Because no significant discontinuity or slope change was observed in the unit-cell volume as a function of pressure across the transition, we also calculated the bulk modulus using all the data for both phases, yielding V_0 = 900.66(2) Å^3, K_0 = 72(1), and K' = 5.7(5). The bulk moduli determined in this study are significantly larger than the value [K_0 = 50(1) GPa with K' = 13(1)] reported by Zhang et al. (1992). The bulk modulus we determined for the 1-K grunerite is 60(2) GPa with V_0 = 920.3(1) Å^3 and K' = 5.5(5). Presumably, the increase in the Fe content would reduce the bulk modulus of cummingtonite and grunerite. The considerably smaller bulk modulus obtained by Zhang et al. (1992) could be due to inconsistent data sets, because they measured the room-pressure unit-cell dimensions from a powder sample but the high-pressure data came from a single crystal. Regardless of the difference in bulk moduli among ferromagnesian cummingtonites, cummingtonite and grunerite appear to be more compressible than calcic-sodic amphiboles. The bulk moduli reported by Comodi et al. (1991) for tremolite, glaucophane, and pargacite are 85, 96, and 97 GPa, respectively. The relatively larger bulk moduli for calcic-sodic amphiboles reflect the importance of the M4 and A cations in the high-pressure crystal-chemistry of the amphibole structures.

Comparison of our high-pressure data with those for a cummingtonite crystal with $X_{Fe} = 0.37$ at low temperature (Yang and Smyth 1996) shows that the volume decrease caused by lowering temperature from room temperature to −133 °C is equivalent to that produced by raising pressure from room pressure to ~0.5 GPa. If we assume that cummingtonite with $X_{Fe} = 0.37$ behaves similarly as that ($X_{Fe} = 0.50$) we studied here, then the crystal studied by Yang and Smyth (1996) would transform from $C2/m$ to $P2_1/m$ symmetry at ~0.2 GPa (Fig. 1).

Structural changes with pressure

Yang and Hirschmann (1995) examined crystal structures of 31 ferromagnesian cummingtonites as a function of composition and found that the A chain in all $P2_1/m$ cummingtonite is always S rotated and the O5-O6-O5 kinking angles in $C2/m$ cummingtonite (~171°) are essentially independent of X_{Fe}. Unlike the effects of changing composition, increasing pressure decreases the kinking angle of the silicate chains in $C2/m$ cummingtonite from 171.2(4)° at room pressure to 169.7(3)° at 1.10 GPa. More importantly, as one crystallographically distinct silicate chain becomes two discontinuously at 1.32 GPa, we found that both A and B chains have the same sense of rotation (O rotation), with the O5-O6-O5 kinking angle of 177.3(9)° for the A chain and 160.5(9)° for the B chain. Furthermore, we observed a change in the sense of rotation for the A chain while the structure retains $P2_1/m$ symmetry: It is O rotated at 1.32 GPa, but S rotated at 2.97 GPa and higher pressures (Fig. 3). This result indicates that the rotation sense of the A chain is independent of the structural symmetry. With increasing pressure, the difference between the kinking angles of the A and B chains ($\Delta\theta$) increases gradually from 16.8° at 1.32 GPa to 42.5° at 7.90 GPa. A similar result has been found as cummingtonite becomes more Mg-rich (Yang and Hirschmann 1995).

Correlated with the variation of the O5-O6-O5 angle with pressure are pronounced changes in some individual M-O bond lengths, especially the M4-O5 and M4-O6 distances (Fig. 4), which are also discontinuous at the transition pressure. The independent adjustments of the A and B chains in the $P2_1/m$ phase evidently modify the coordination of the M4 site. Between room pressure and 1.10 GPa, the M4 cation has four O atoms within a radius of 3.0 Å (two O2 and two O4) at a distance < 2.20 Å and two O6 atoms at a distance > 2.60 Å (the M4-O5 dis-

TABLE 5. Polyhedral volumes (Å^3) and distortion indices of cummingtonite at various pressures

				1.32		2.97	
P (GPa)	0.00	0.60	1.10	Set A	Set B	Set A	Set B
M1 V*	12.41(4)	12.37(4)	12.43(4)	12.39(13)		12.28(8)	
M1 QE	1.0091(4)	1.0083(3)	1.0076(3)	1.0091(10)		1.0067(6)	
M1 AV	29.2(6)	26.9(5)	24.5(5)	24.3(1.5)		20.9(9)	
M2 V	12.09(4)	12.18(4)	12.17(4)	12.09(14)		11.87(8)	
M2 QE	1.0098(3)	1.0090(3)	1.0078(3)	1.0092(10)		1.0082(6)	
M2 AV	32.9(5)	29.9(5)	25.9(4)	31.2(1.6)		26.6(9)	
M3 V	12.12(5)	12.08(4)	12.21(4)	12.12(15)		11.94(10)	
M3 QE	1.0135(4)	1.0121(4)	1.0108(3)	1.0147(14)		1.0087(7)	
M3 AV	44.5(6)	39.8(6)	35.7(5)	44.8(2.2)		29.1(1.2)	
M4 V^{VI}†	11.60(4)	11.52(4)	11.42(3)	11.33(11)		11.10(7)	
M4 QE	1.2484(13)	1.2574(12)	1.2624(13)	1.2709(40)		1.2765(28)	
M4 AV	447.0(9)	455.5(9)	461.1(9)	473.1(2.9)		485.2(2.0)	
M4 V^{VIII}†	24.53(6)	24.42(6)	24.19(6)	24.13(19)		23.42(12)	
T1 V	2.18(1)	2.17(1)	2.15(1)	2.21(3)	2.17(3)	2.13(2)	2.22(2)
T1 QE	1.0085(1)	1.0003(1)	1.0004(1)	1.0011(5)	1.0042(11)	1.0010(3)	1.0013(4)
T1 AV	2.3 (3)	1.2(2)	1.3(2)	3.1(8)	13.7(21)	3.8(6)	4.1(7)
T2 V	2.20(1)	2.16(1)	2.16(1)	2.15(3)	2.15(4)	2.19(2)	2.10(2)
T2 QE	1.0048(4)	1.0048(3)	1.0046(3)	1.0065(14)	1.0060(14)	1.0073(9)	1.0042(6)
T2 AV	19.4(7)	19.7(7)	18.6(6)	22.8(2.7)	19.0(2.7)	30.0(1.9)	14.2(1.2)

* V = polyhedral volume; QE = polyhedral quadratic elongation; AV = polyhedral angle variance (Robinson et al. 1971).
† V^{VI} = sixfold-coordinated volume; V^{VIII} = eightfold-coordinated volume.

tance is greater than 3.10 Å). However, as a consequence of the increased kinking of the silicate chains at higher pressures, the M4 cation in the $P2_1/m$ structure becomes sevenfold-coordinated: The O5B atom also moves into the coordination sphere whereas the O5A atom moves far away (Fig. 5). In fact, the configuration of the M4 site at 1.32 and 2.97 GPa resembles that in anthophyllite (Finger 1970), which has a sevenfold coordination for the M4 site at ambient conditions. More interestingly, the M4-O5B distance reduces appreciably from 2.944 to 2.551 Å as pressure is raised from 1.32 to 7.90 GPa, whereas the M4-O6B distance increases from 2.754 to 2.903 Å (Fig. 5). In other words, there is a switching of the nearest bridging O atoms coordinated with the M4 cation. [Similar results have been reported for several clinopyroxenes (Brown et al. 1972; Smyth 1974; Sueno et al. 1984) and Fe-bearing orthopyroxenes (Smyth 1973; Sueno et al. 1976; Yang and Ghose 1995) owing to the pronounced straightening of the silicate chains at high temperatures.] The pressure at which the M4-O5B distance becomes shorter than the M4-O6B distance is between 1.32 and 2.97 GPa. Because of the moving in of the O5B atom into the M4-cation coordination sphere at higher pressures, the number of the shared edges for the M4 polyhedron increases from five in the $C2/m$ structure to six in the $P2_1/m$ structure. Between room pressure and 1.10 GPa, the M4 cation shares three edges with the surrounding octahedra (one with M1 and two with M2) and two edges with the T2 tetrahedra, whereas it shares an additional edge with T1B tetrahedron between 1.32 and 7.90 GPa. Energetically, such a polyhedral configuration in the $P2_1/m$ phase is unstable because of the strong parity violation. This may explain why the high-pressure $P2_1/m$ structure reversibly inverts back to the $C2/m$ structure when the pressure is released.

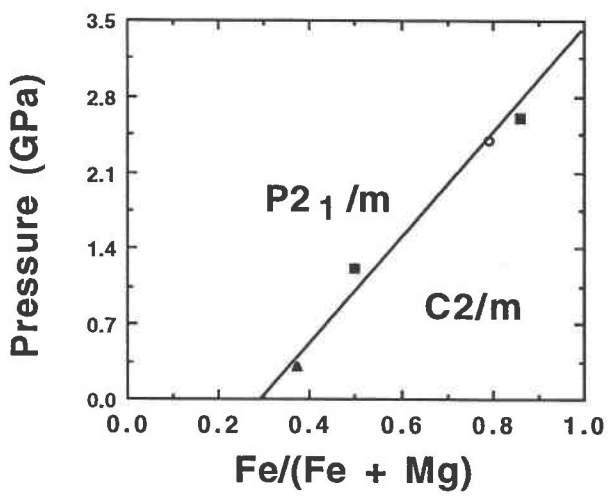

FIGURE 1. $C2/m$-$P2_1/m$ phase-transition pressure (P_{tr}) as a function of bulk composition [Fe/(Fe + Mg)] in cummingtonite/grunerite. Solid squares = P_{tr} determined in this study; open circle = estimated P_{tr} for grunerite studied by Zhang and Hafner (1992) and Zhang et al. (1992); solid triangle = estimated P_{tr} for cummingtonite studied by Yang and Smyth (1995).

Various cation polyhedra respond differently to high pressure. Between room pressure and 1.10 GPa, volumes of the M1, M2, and M3 octahedra in the $C2/m$ structure do not change significantly, whereas those of the empty A and the highly distorted M4 polyhedra reduce by 3.1 and 1.4%, respectively, yielding a bulk modulus of 35(4) GPa for the A site and 71(8) GPa for the M4 site. Relative

TABLE 5—*Extended*

	5.09		7.90	
P (GPa)	Set A	Set B	Set A	Set B
M1 V	12.00(8)		11.80(6)	
M1 QE	1.0062(6)		1.0054(4)	
M1 AV	20.5(9)		17.9(7)	
M2 V	11.60(7)		11.34(6)	
M2 QE	1.0074(5)		1.0067(4)	
M2 AV	24.7(8)		22.2(7)	
M3 V	11.69(9)		11.54(7)	
M3 QE	1.0085(7)		1.0070(5)	
M3 AV	28.3(1.1)		23.5(8)	
M4 V^{VI}	10.81(7)		10.55(6)	
M4 QE	1.2876(30)		1.3012(23)	
M4 AV	500.7(2.0)		625.6(1.9)	
M4 V^{VIII}	22.62(11)		22.08(10)	
T1 V	2.17(2)	2.17(2)	2.15(2)	2.15(2)
T1 QE	1.0014(4)	1.0005(2)	1.0015(4)	1.0014(2)
T1 AV	6.1(9)	1.7(4)	6.5(8)	2.5(4)
T2 V	2.10(2)	2.17(2)	2.11(2)	2.14(2)
T2 QE	1.0071(8)	1.0032(5)	1.0076(7)	1.0031(4)
T2 AV	28.6(1.7)	11.9(9)	31.0(1.5)	7.8(7)

to those in the *C2/m* phase, the A and M4 polyhedra in the $P2_1/m$ phase are less compressible, with bulk moduli of 52(4) and 96(7) GPa, respectively. Within the experimental uncertainties, the M1, M2, and M3 octahedra in the $P2_1/m$ structure exhibit similar compressibilities: Their respective volumes reduce by 4.9, 6.2, and 4.8%, and their bulk moduli are 134(12), 107(7), and 137(17) GPa. The high-pressure structural study of Comodi et al. (1991) on tremolite, pargasite, and glaucophane reveals the similar compressible trend for various polyhedra as we determined, with the A polyhedron being the softest regardless of its vacancy or occupation by large cations, followed by M4 and by M1-M2-M3. Comodi et al. (1991) attributed the greatest compressibility of the calcic-sodic amphibole structures along [100] to the softness of the A polyhedron, which occurs between two I-beams along [100] (see Cameron and Papike 1979 for illustrations of I-beam diagrams for the amphibole structures). In cummingtonite, the A site is empty, and thus the softest; hence, its high-pressure behavior controls the compression of the structure. However, preferential compression of the A polyhedron appears to be only dominant in the *C2/m* structure. After the collapse of the A cavity and the structural modification from *C2/m* to $P2_1/m$ symmetry, the behavior of the M polyhedra also becomes an important factor in determining the compression of the structure.

With increasing pressure, the M1, M2, and M3 octahedra in both *C2/m* and $P2_1/m$ polymorphs become more regular, whereas the M4 octahedron becomes progressively more distorted both in bond lengths and angular distortion, assuming that the M4 cation is always coordinated by two O2, two O4, and two O6 atoms as it is at room pressure (Table 5). However, if we consider only six nearest O atoms as coordinated to the M4 cation at higher pressures, then the distortion of the M4 octahedron

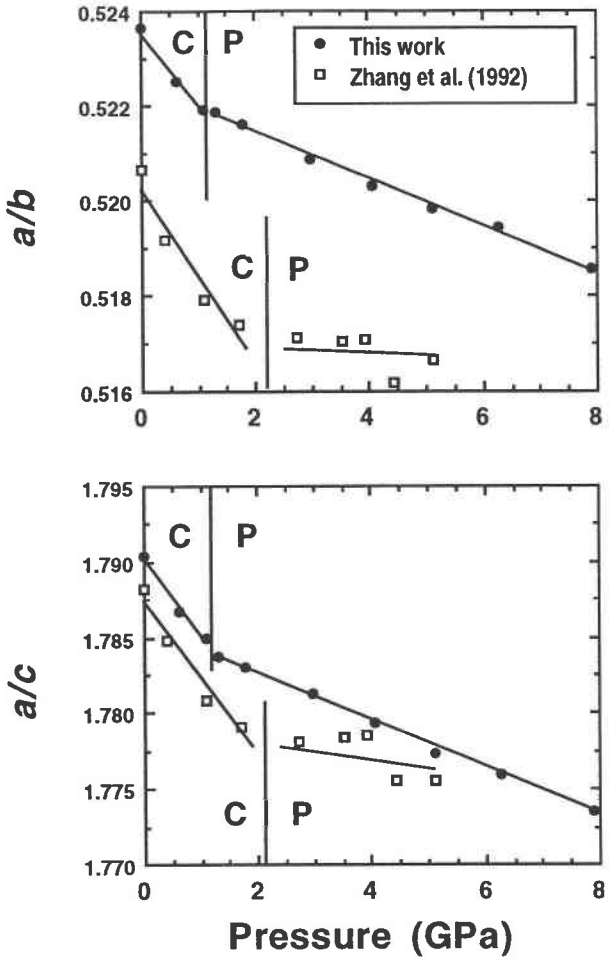

FIGURE 2. Axial ratios *a/b* and *a/c* vs. pressure. Abbreviations: C = *C2/m* and P = $P2_1/m$.

decreases considerably with increasing pressure, due to the switching of the O6B and O5B atoms. For example, the octahedral angle variance (OAV) (Robinson et al. 1971) for the M4 octahedron is 447(1) at room pressure, whereas it is 201(2) at 7.90 GPa. These results are comparable to the high-pressure Mössbauer spectra measured by Zhang and Hafner (1992), who interpreted their data as a consequence of increasing distortion in the M1, M2, and M3 octahedra and decreasing distortion in the M4 octahedron.

Among various cation polyhedra, the T1 and T2 tetrahedra are the most incompressible. Between room pressure and 7.90 GPa, their respective volumes (the average of the TA and TB volumes for the $P2_1/m$ structure) reduce only by 1.4 and 3.0%, yielding a bulk modulus of 564 (158) GPa for T1 and 354(124) GPa for T2. The relative rigid behavior of the SiO_4 groups is expected, given the Si-O bond strength and the large flexibility of the structure.

There is a systematic increase in the β angle with increasing pressure, an observation contrasting to that

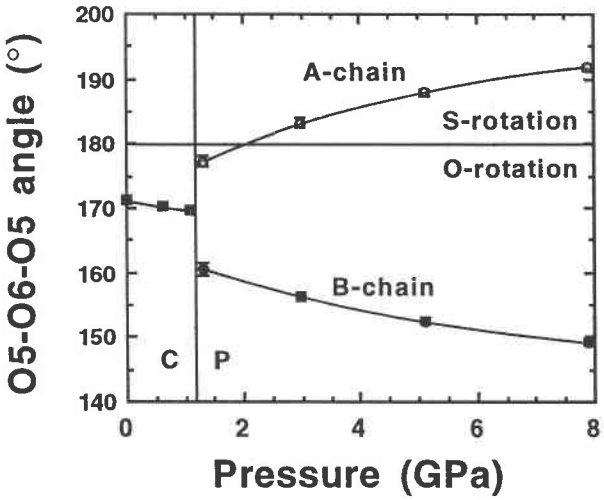

FIGURE 3. O5-O6-O5 kinking angles in cummingtonite as a function of pressure. The kinking angle of the A chain is plotted as 360° minus the O5A-O6A-O5A angle to maintain the analogy with pyroxenes. Note the same rotation sense of the A and B chains at 1.32 GPa.

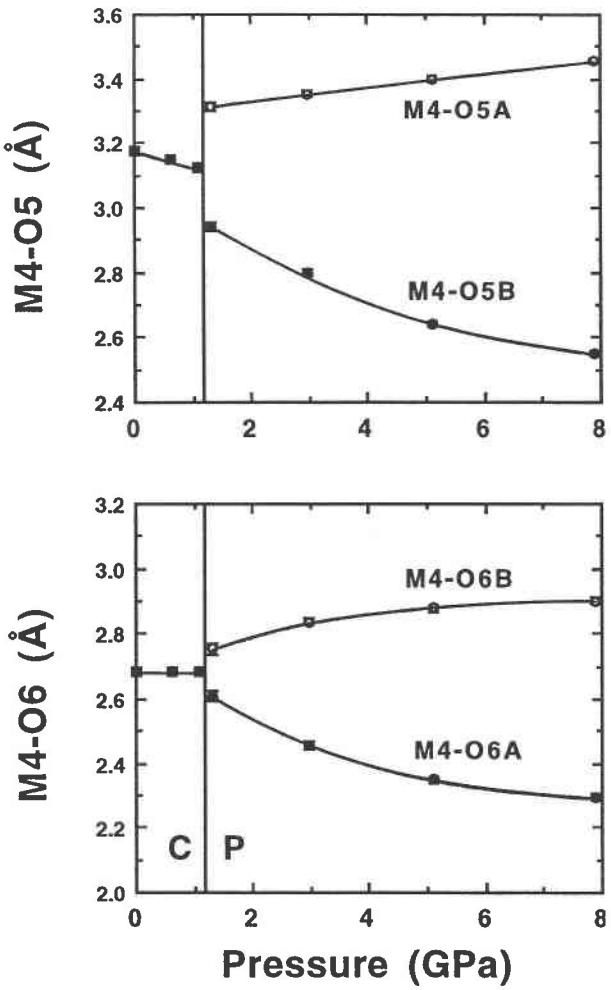

FIGURE 4. Variations of the M4-O5 and M4-O6 distances in cummingtonite with pressure.

caused by increasing temperature (Sueno et al. 1972) or chemical expansion in which larger β angles correspond to larger M4-cations [or macroscopic Fe/(Fe + Mg)] (Hirschmann et al. 1994). Whittaker (1960) correlated the β angle in amphibole to the relative arrangement of the adjacent silicate chains. By defining the distance between the center of the two opposing six-membered tetrahedral rings as the chain displacement factor (CDF), Sueno et al. (1973) found a negative linear correlation between CDF and the β angle for various amphiboles as a function of temperature and chemical composition. A plot of the β angle vs. the calculated CDF values at various pressures also shows a good negative linear relationship (Fig. 6), suggesting that increasing pressure decreases the relative displacement of the adjacent silicate chains in cummingtonite. According to Whittaker (1960), a reduction in the relative displacement of the two opposing silicate chains results in a decrease in the degree of the closest packing of the tetrahedral chains.

High-pressure infrared spectra

At room pressure, four bands of the OH stretching vibration in cummingtonite were observed in the near-infrared region at ~3618, 3638, 3654, and 3667 cm^{-1} (Fig. 7). These four bands are labeled as A, B, C, and D from high to low frequency and correspond to the respective cation configurations of 3Mg, 2Mg/Fe, Mg/2Fe, and 3Fe among the one M3 and two M1 sites [see Hawthorne (1983) for a review of the nomenclature and assignment of bands]. The full width at half maximum (FWHM) of these bands are fairly narrow ranging from 4 to 8 cm^{-1}. The separation among the bands is larger toward the 3Fe configuration.

On compression, a splitting in four bands occurred between 1.04 and 1.54 GPa, indicating a structural modification at ~1.29 ± 0.25 GPa, in agreement with the X-ray diffraction measurement. The amount of splitting between the two sets of fourfold bands is approximately constant (~4 cm^{-1}) between 1.54 and 8.63 GPa. Such a moderate splitting (smaller than the FWHMs of the original four bands) leads to slightly overlapping but resolvable bands for the $P2_1/m$ polymorphs. Frequency shifts

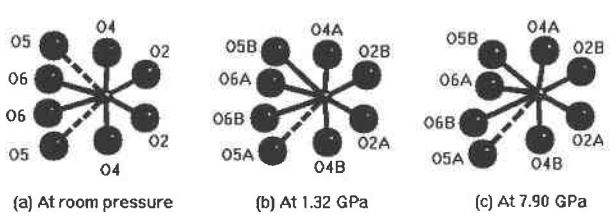

FIGURE 5. Atomic coordination for the M4 cation in cummingtonite: (**a**) at room pressure, (**b**) at 1.32 GPa, and (**c**) at 7.90 GPa. The distances connected by solid lines are within 3.0 Å and the dashed lines beyond 3.0 Å.

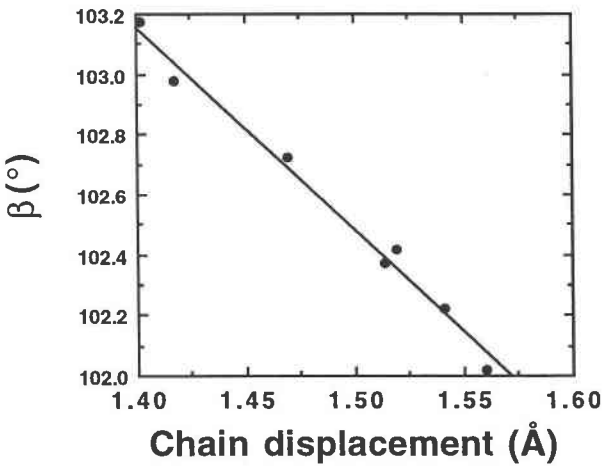

FIGURE 6. Relationship between the β angle and chain displacement factor in cummingtonite.

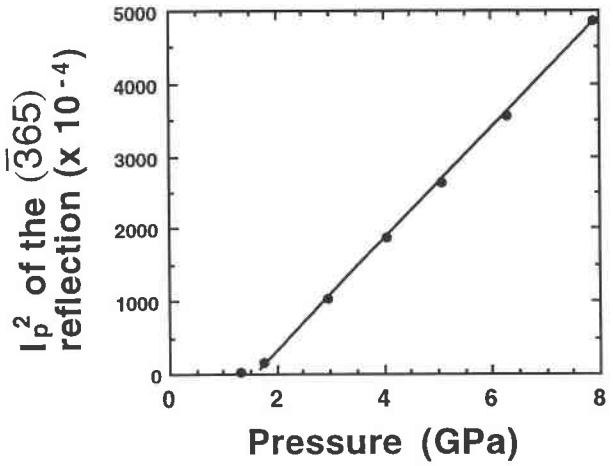

FIGURE 8. Squared intensity of the primitive $(\bar{3}65)$ reflection as a function of pressure.

of the bands with increasing pressure are nearly linear and range from −0.14 to +1.22 cm^{-1}/GPa with the lowest corresponding to the 3Fe configuration and the highest to the 3Mg configuration.

From the crystal-structural point of view, the splitting of the OH stretching vibrational bands across the *C*2/*m*-*P*2$_1$/*m* transition is expected because there is only one crystallographically distinct OH position (O3-H) in the *C*2/*m* structure, but there are two in the *P*2$_1$/*m* structure. The different environments of two OH positions in the *P*2$_1$/*m* phase give rise to the difference in the stretching frequencies, resulting in the splitting of the hydroxyl bands. Our high-pressure infrared spectroscopic results are comparable to the low-temperature Raman spectra measured by Wang et al. (1988), who observed a significant broadening, but not splitting, of the B and C bands for a cummingtonite sample with X_{Fe} = 0.39 as temperature was decreased from 295 to 83 K. The band broadening observed by Wang et al. (1988) was ascribed to the *C*2/*m*-to-*P*2$_1$/*m* phase transformation by Yang and Smyth (1996).

The pressure derivatives of OH stretching frequencies of four bands indicate that the H-Mg and H-Fe structural environments show contrasting behavior. The slightly

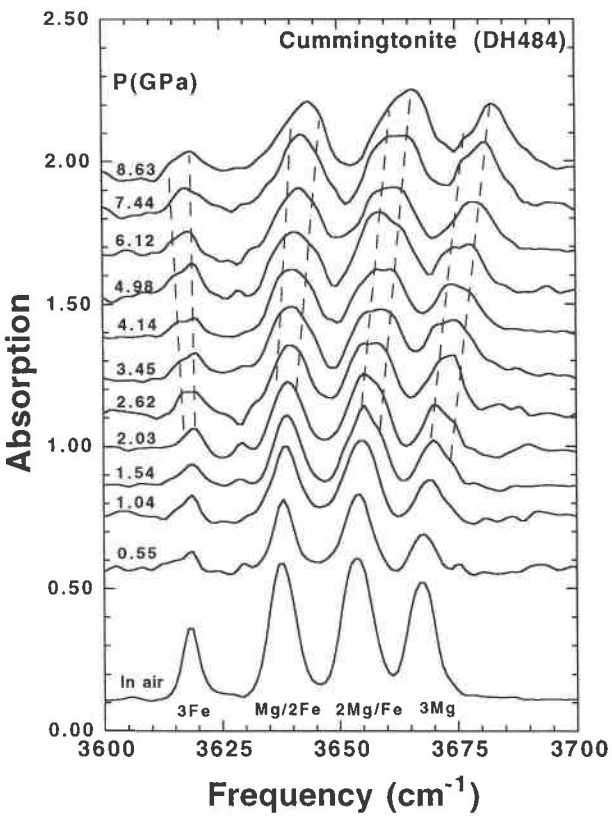

FIGURE 7. Infrared spectra of cummingtonite at high pressure in the OH stretching region. Spectra are displaced along the vertical axis for clarity.

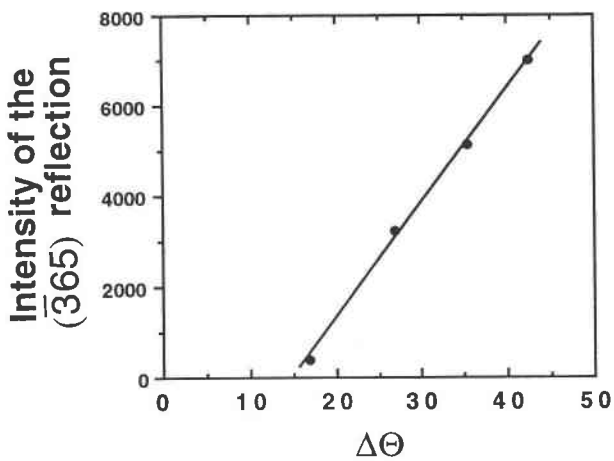

FIGURE 9. The intensity of the primitive $(\bar{3}65)$ reflection vs. the difference between the kinking angles of the A and B chains (Δθ).

negative frequency shift for the 3Fe configuration indicates that there is only a weak component of hydrogen bonding in this system and the bonding nature is predominately normal hydroxyl bonding. Thus, the larger and positive frequency shift toward the 3Mg configuration is likely associated with a greater compressibility of the H-Mg configuration than the H-Fe configuration, rather than arising from the difference in the hydrogen bonding of the two configurations.

Nature of the *C2/m-P2$_1$/m* phase transition

Many similarities exist between clinopyroxene and clinoamphibole crystal structures (e.g., Hawthorne 1983; Yang and Hirschmann 1995) and phase-transition mechanisms (Prewitt et al. 1970; Sueno et al. 1972; Carpenter 1982). It is, therefore, intriguing to see whether or not the two major groups of rock-forming chain silicates have a similar phase-transition nature. From high-temperature single-crystal X-ray diffraction, Smyth (1974) showed that *P2$_1$/c-C2/c* transformation in clinohypersthene is of first-order in character and the kinking angles of two nonequivalent single-silicate chains behave similarly as we observed for cummingtonite. Further evidence for the first-order transition in clinoenstatite and pigeonite was provided by Shimobayashi and Kitamura (1991) from in-situ high-temperature transmission electron microscopy, who observed the coexistence of both *C2/c* and *P2$_1$/c* phases separated by sharp interfaces and nucleation-growth process, a characteristic of the first-order phase transition. Although the unit-cell dimensions with pressure for cummingtonite (this study) and grunerite (Zhang et al. 1992) do not show an obvious discontinuity, our structural data clearly indicate an abrupt change in some structural parameters across the *C2/m-P2$_1$/m* transition, such as the O5-O6-O5 kinking angles and the M4-O5 and M4-O6 bond lengths. Therefore, the *C2/m-P2$_1$/m* phase transition in cummingtonite likely has weakly displacive first-order character. A plot of the squared intensity of a primitive reflection (I_p^2) against pressure shows that I_p^2 is proportional to ($P - P_{tr}$) between 1.76 and 7.90 GPa, but appears to deviate slightly from the linear relationship between 1.32 and 1.76 GPa (Fig. 8). This small deviation could stem from the possible presence of defects or domains in the cummingtonite structure (Salje 1990). In general, the intensity of a superlattice reflection is proportional to the square of the order parameter (Q^2) (Bruce and Cowley 1981). Thus, our data imply that Q is proportional to $(P - P_{tr})^{\beta}$ with $\beta = 1/4$. According to Landau theory, this suggests a tricritical character for the structural transformation in cummingtonite—a phase transition that is between discontinuous (first-order) and continuous (second-order).

In the *C2/m* cummingtonite structure, the M4 cation is situated at the periphery of the octahedral strip formed by the M1, M2, and M3 octahedra and cross-linked to two back-to-back double silicate chains that are related by a twofold symmetry operation. As shown above, the M4 site is the most compressible of all occupied polyhedra, whereas the SiO_4 tetrahedra are the least compressible. Thus, there exists a mismatch between the compressibilities of the M4 and T sites. To reduce such a mismatch, the structure responds by the relative tilting of the SiO_4 tetrahedra or the increase in the kinking of the silicate chains as pressure increases. At ~1.21 GPa, however, the simultaneous kinking of the two symmetry-related tetrahedral chains can no longer offset the differential compression between the M4 and T sites. As a consequence, the twofold symmetry that relates the two back-to-back chains is broken (but the twofold screw axis remains), and the M4 site collapses, giving rise to the *P2$_1$/m* structure. In other words, the *C2/m-P2$_1$/m* phase transition in cummingtonite is primarily driven by the differential compression between the M4 site and the SiO_4 tetrahedra, and the relaxation in symmetry constraints (from *C2/m* to *P2$_1$/m*) is to provide a necessary tighter coordination for the M4 site. Such a mechanism suggests that the high-pressure behavior of the M4 site controls the nature of the phase transition in cummingtonite and grunerite solid solutions. Because the chemical substitution at the M4 site (for example, Mn for Fe) will affect the high-pressure behavior of the M4 polyhedron, we might expect the phase-transition character vary with composition. From the above discussion, we can also expect a correlation between the intensity of a primitive reflection (I_p) and the difference between the kinking angles of the A and B chains ($\Delta\theta$). As demonstrated in Figure 9, there is an excellent linear relationship between the two parameters. As I_p is proportional to Q^2, Figure 9 indicates a linear-quadratic coupling of $\Delta\theta$ to the order parameter.

Hazen and Finger (1979) reviewed solid-solid phase transitions due to polyhedral tilt and concluded that these structural transformations mainly occur in compounds with structures composed of corner-linked, rigid polyhedral elements and are reversible and nonquenchable with lower-symmetry structures more distorted. The phase transition in cummingtonite satisfies these criteria and, thus, can be considered as a polyhedral tilt transition, a subgroup of pure displacive phase transformations.

Acknowledgments

We thank B.W. Evans of the University of Washington for providing us with the DH7-484 and 1-K samples and H.K. Mao for helpful discussions. X-ray diffraction work and postdoctoral fellowship to H.Y. at the Geophysical Laboratory are supported by NSF grant EAR-9218845, the Center for High Pressure Research, and by the Carnegie Institution of Washington. Infrared measurements were supported by NSF grant EAR-9526763 and DOE grant DE-FG02-96ER14651.

References cited

Becker, P.J. and Coppens, P. (1975) Extinction within the limit of validity of the Darwin transfer equations: III. Non-spherical crystals and anisotropy of extinction. Acta Crystallographica, A31, 417–425.

Brown, G.E., Prewitt, C.T., Papike, J.J., and Sueno, S. (1972) A comparison of the structures of low and high pigeonite. Journal of Geophysical Research, 77, 5778–5789.

Bruce, A.D. and Cowley, R.A. (1981) Structural phase transitions, p. 326. Taylor and Francis, London.

Cameron, M. and Papike, J.J. (1979) Amphibole crystal chemistry: A review. Fortschritte der Mineralogie, 57, 28–67.

Carpenter, M.A. (1982) Amphibole mircostructures: some analogies with phase transformations in pyroxenes. Mineralogical Magazine, 46, 395–397.

Chisholm, J.E. (1981) Pyribole structure types. Mineralogical Magazine, 44, 205–216.

Comodi, P., Mellini, M., Ungaretti, L., and Zanazzi, P.F. (1991) Compressibility and high pressure structure refinement of tremolite, pargasite and glaucophane. European Journal of Mineralogy, 3, 485–499.

Finger, L.W. (1969) The crystal structure and cation distribution of a grunerite. Mineralogical Society of America Special Paper, 2, 95–100.

———(1970) Refinement of the crystal structure of an anthophyllite. Carnegie Institution of Washington Yearbook, 68, 283–288.

Finger, L.W. and King, H. (1978) A revised method of operation of the single-crystal diamond cell and refinement of the structure of NaCl at 32 kbar. American Mineralogist, 63, 337–342.

Finger, L.W. and Prince, E. (1975) A system of FORTRAN IV computer programs for crystal structure computations. National Bureau of Standards Technology Note 854.

Hawthorne, F.C. (1983) Crystal chemistry of the amphiboles. Canadian Mineralogist, 21, 173–480.

Hazen, R.M. and Finger, L.W. (1979) Polyhedral tilting: A common type of pure displacive phase transition and its relationship to analcite at high pressure. Phase Transitions, 1, 1–22.

Hirschmann, M., Evans, B.W., and Yang, H. (1994) Composition and temperature dependence of Fe-Mg ordering in cummingtonite-grunerite as determined by X-ray diffraction. American Mineralogist, 79, 862–877.

Ibers, J.A. and Hamilton, W.C., Eds. (1974) International tables for X-ray crystallography. vol. IV, 366 p. Kynoch, Birmingham, U.K.

King, H.E. and Finger, L.W. (1979) Diffracted beam crystal centering and its application to high pressure crystallography. Journal of Applied Crystallography, 12, 374–378.

Law, A.D. and Whittaker, E.J.W. (1980) Rotated and extended model structures in amphiboles and pyroxenes. Mineralogical Magazine, 43, 565–574.

Lehmann, M.S. and Larsen, F.K. (1974) A method for location of the peaks in step-scan-measured Bragg reflexions. Acta Crystallographica, A30, 580–584.

Mao, H.K. and Hemley, R.J. (1996) Experimental studies of Earth's deep interior: Accuracy and versatility of diamond-anvil cells. Philosophical Transactions of the Royal Society London, Series A, 354, 1315–1332.

Mao, H.K., Xu, J., and Bell, P.M. (1986) Calibration of the ruby pressure gauge to 800 kbar under quasi-hydrostatic conditions. Journal of Geophysical Research, 91, 4673–4676.

Maresch, W.V. and Czank, M. (1988) Crystal chemistry, growth kinetics and phase relationships of structurally disordered (Mn^{2+}–Mg)-amphiboles. Fortschritte der Mineralogie, 66, 69–121.

Mueller, R.F. (1960) Compositional characteristics and equilibrium relations in mineral assemblages based on a metamorphosed iron formation. American Journal of Science, 258, 449–497.

Papike, J.J. and Ross, M. (1970) Gedrites: Crystal structures and intracrystalline cation distributions. American Mineralogist, 55, 1945–1972.

Papike, J.J., Ross, M., and Clark, J.R. (1969) Crystal-chemical characterization of clinoamphiboles based on five new structure refinements. Mineralogical Society of America Special Paper, 2, 117–137.

Prewitt, C.T., Papike, J.J., and Ross, M. (1970) Cummingtonite: A reversible nonquenchable transition from $P2_1/m$ to $C2/m$ symmetry. Earth and Planetary Science Letters, 8, 448–450.

Prewitt, C.T., Brown, G.E., and Papike, J.J. (1971) Apollo 12 clinopyroxenes: High temperature X-ray diffraction studies. Geochimca et Cosmochimca Acta, Supplement 2, 1, 59–68.

Robinson, K., Gibbs, G.V., and Ribbe, P.H. (1971) Quadratic elongation: A quantitative measure of distortion in coordination polyhedra. Science, 172, 567–570.

Ross, M., Papike, J.J., Shaw, K.W., and Weiblen, P.W. (1968) Exsolution in clinoamphiboles. Science, 159, 1099–1102.

Ross, M., Papike, J.J., and Shaw, K.W. (1969) Exsolution textures in amphiboles as indicators of subsolidus thermal histories. Mineralogical Society of America Special Paper, 2, 275–299.

Salje, E.K.H. (1990) Phase transitions in ferroelastic and co-elastic crystals, p. 366. Cambridge University Press, New York.

Shimobayashi, N. and Kitamura, M. (1991) Phase transition in Ca-poor clinopyroxenes: A high temperature transmission electron miroscopic study. Physics and Chemistry of Minerals, 18, 153–160.

Smyth, J.R. (1973) An orthopyroxene structure up to 850°C. American Mineralogist, 58, 636–648.

———(1974) The high temperature crystal chemistry of clinohypersthene. American Mineralogist, 59, 1069–1082.

Smyth, J.R. and Burnham, C.W. (1972) The crystal structures of high and low clinohypersthene. Earth and Planetary Science Letters, 14, 183–189.

Sueno, S., Papike, J.J., Prewitt, C.T., and Brown, G.E. (1972) Crystal chemistry of high cummingtonite. Journal of Geophysical Research, 77, 5767–5777.

———(1973) The high temperature crystal chemistry of tremolite. American Mineralogist, 58, 649–664.

Sueno, S., Cameron, M., and Prewitt, C.T. (1976) Orthoferrosilite: High-temperature crystal chemistry. American Mineralogist, 61, 38–53.

Sueno, S., Kimata, M., and Prewitt, C.T. (1984) The crystal structure of high clinoferrosilite. American Mineralogist, 69, 264–269.

Veblen, D.R. (1985) Non-classical pyriboles and polysomatic reactions in biopyriboles. In Mineralogical Society of America Reviews in Mineralogy, 9A, 189–236.

Wang, A., Dhamelincourt, P., and Turrell, G. (1988) Infrared and low-temperature micro-Raman spectra of the OH stretching vibrations in cummingtonite. Applied Spectroscopy, 42, 1451–1457.

Whittaker, E.J.W. (1960) The crystal chemistry of amphiboles. Acta Crystallographica, 13, 291–298.

Yang, H. and Ghose, S. (1995) A transitional structural state and anomalous Fe-Mg order-disorder in Mg-rich orthopyroxene, $(Mg_{0.75}Fe_{0.25})_2Si_2O_6$. American Mineralogist, 80, 9–20.

Yang, H. and Hirschmann, M.M. (1995) Crystal structure of $P2_1/m$ ferromagnesian amphibole and the role of cation ordering and composition in the $P2_1/m$-$C2/m$ transition in cummingtonite. American Mineralogist, 80, 916–922.

Yang, H. and Smyth, J.V. (1996) Crystal structure of a $P2_1/m$ ferromagnesian cummingtonite at 140 K. American Mineralogist, 81, 363–368.

Zhang, L. and Hafner, S.S. (1992) Gamma resonance of ^{57}Fe in grunerite at high pressures. American Mineralogist, 77, 474–479.

Zhang, L., Ahsbahs, H., Kutoglu, A., and Hafner, S.S. (1992) Compressibility of grunerite. American Mineralogist, 77, 480–483.

Manuscript received June 10, 1997
Manuscript accepted November 10, 1997